Nonlocal microscopic theory of quantum friction between parallel metallic slabs

Despoja, Vito; Echenique, Pedro M.; Šunjić, Marijan

Nonlocal microscopic theory of quantum friction between parallel metallic slabs

Vito Despoja,[1,2,3] Pedro M. Echenique,[1,3] and Marijan Šunjić[1,2]

[1]*Donostia International Physics Center (DIPC), P. Manuel de Lardizabal, E-20018 San Sebastian, Basque Country, Spain*

[2]*Department of Physics, University of Zagreb, Bijenička 32, HR-10000 Zagreb, Croatia*

[3]*Departamento de Fisica de Materiales and Centro Mixto CSIC-UPV/EHU, Facultad de Ciencias Quimicas, Universidad del Pais Vasco UPV/EHU, Apto. 1072, E-20080 San Sebastian, Basque Country, Spain*

(Received 13 December 2010; revised manuscript received 8 April 2011; published 23 May 2011)

We present a new derivation of the friction force between two metallic slabs moving with constant relative parallel velocity, based on $T = 0$ quantum-field theory formalism. By including a fully nonlocal description of dynamically screened electron fluctuations in the slab, and avoiding the usual matching-condition procedure, we generalize previous expressions for the friction force, to which our results reduce in the local limit. Analyzing the friction force calculated in the two local models and in the nonlocal theory, we show that for physically relevant velocities local theories using the plasmon and Drude models of dielectric response are inappropriate to describe friction, which is due to excitation of low-energy electron-hole pairs, which are properly included in nonlocal theory. We also show that inclusion of dissipation in the nonlocal electronic response has negligible influence on friction.

DOI: 10.1103/PhysRevB.83.205424 PACS number(s): 68.35.Af, 61.85.+p, 73.20.Mf

I. INTRODUCTION

Energy of a charged or neutral particle (e.g., electron or atom) at rest or slowly moving close to a dielectric surface, e.g., parallel to a metallic slab,[1–6] is shifted downward, because of its interaction with the quantum-mechanical charge-density fluctuations in the system via nonretarded Coulomb interaction (at close distances), leading to dynamical image or van der Waals potentials, respectively. Parallel velocity leads to a typical Doppler-shifted frequency in the resulting expressions. For higher velocities real electronic transitions, in the slab as well as in the particle, can occur and a moving particle starts losing kinetic energy and parallel momentum. In the past decade, much attention has been paid to a similar dissipative phenomenon, the so-called quantum or van der Waals friction, i.e., frictional forces between two parallel dielectrics without direct contact moving with parallel velocity, at zero or finite temperature. This is not only an intriguing theoretical problem, but also potentially relevant phenomenon, e.g., affecting the behavior of micromechanical devices, so-called Micro-Electro-Mechanical Systems (MEMS),[7–9] of nanometer dimensions. In this situation, an obvious question can be posed: is this process physically feasible, since translation symmetry is not broken and dielectrics are not in contact, and, if it is, which mechanism is responsible for friction?

A number of authors approached this question[10–20] with different and often contradictory conclusions, even questioning the possibility of quantum friction[20,21] as formulated by Pendry[14] in spite of several extensive studies, e.g., by Persson and Volokitin.[15–18,22,23] In order to ellucidate this question, we here provide a new derivation of energy dissipation rate and quantum friction using a completely nonlocal description of the dynamical response of a metallic slab. The resulting expressions are formally the same, but instead of surface reflectivities derived by the field matching conditions at metallic surfaces, our results contain microscopically calculated generalized surface reflectivities, which are directly related to surface plasmon propagators. In this way, we do not depend, e.g., on the form of a local dielectric function nor on the assumption of sharp charge-density profiles.

In Sec. II, we present our derivation of the energy dissipation rate and friction force, based on the nonlocal dynamical response functions of the slabs, and discuss their connection with the previous results to which they reduce in the long-wavelength (local) limit.

In Sec. III, we discuss the obtained results and the problems of introducing nonlocality in the description of Electro-Magnetic (EM) fields in finite systems, emphasizing the advantage of our microscopic formulation of surface reflectivities.

In Sec. IV, we calculate the velocity dependence of the friction force between two finite metallic slabs at $T = 0$ in two local approximations, i.e., using the plasmon and Drude models, and in a fully nonlocal theory. In this latter case, we use the surface plasmon propagators, which are the same as the ones in the nonlocal theory of van der Waals forces.[24] We show that these local models lead to friction only at physically irrelevant, i.e., extremely high velocities, while at lower velocities they give negligible results. At these lower velocities, the main contribution to friction comes from the excitation of electron-hole pairs, which are absent in the local models, but correctly described in our nonlocal theory.

It should be pointed out that our main goal is to discuss the effects of spatial dispersion and especially electron-hole excitations and not the dissipation, even if it is present in real systems. For comparison with our results, it is therefore appropriate to use the local (dissipationless) plasmon model, i.e., the Drude model without dissipation.

However, to clarify the role of dissipation, and in order to compare the Drude model with phenomenological damping constant with our results, we also introduce the same damping in nonlocal response function. We calculate the excitation spectra and friction in all these cases and show that the low-energy friction remains practically unchanged, while the Drude model gives negligible results.

In Sec. V, we present the conclusions.

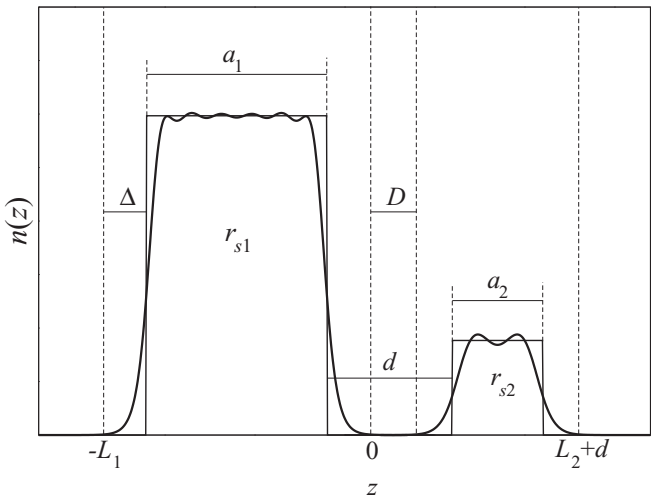

FIG. 1. Density profile for two nonoverlapping metallic slabs.

II. THEORETICAL FORMULATION

In this section, we present a new microscopic derivation of the quantum friction between two parallel metallic (dielectric) slabs (Fig. 1) moving in parallel direction with relative velocity $\mathbf{v}$. We shall treat the nonretarded case at zero temperature and describe charge fluctuations in the slabs microscopically, i.e., using a fully nonlocal response function. This means that we shall not rely on the local description of the induced electromagnetic fields in a system with sharp boundaries and local dielectric functions. In this way, we do not have to use matching conditions at the slab boundaries, which will enable us to treat arbitrary (smooth) electron-density profiles. Also, most importantly, the metallic response will include not only plasmon excitations, already included in the local dielectric function, but also soft electron-hole pairs, which give the dominant contribution to energy dissipation.

We start by considering some external dynamical charge distribution close to some polarizable and dissipative system. The rate at which the external charge is losing energy and heating the system can be written as[1,2]

$$P(t) = \int d\mathbf{r}\, \mathbf{E}^{\rm ext}(\mathbf{r},t)\mathbf{j}^{\rm ind}(\mathbf{r},t), \tag{1}$$

where $\mathbf{E}^{\rm ext}$ is the electrical field produced by the external charge and $\mathbf{j}^{\rm ind}(\mathbf{r},t)$ is the induced current in the system. After using $\mathbf{E}^{\rm ext} = -\nabla\phi^{\rm ind}$ and the continuity Eq. (1) can also be written as

$$P(t) = \int d\mathbf{r}\, \rho^{\rm ext}(\mathbf{r},t)\frac{d}{dt}\phi^{\rm ind}(\mathbf{r},t). \tag{2}$$

If we express the induced potential $\phi^{\rm ind}$ as

$$\phi^{\rm ind}(\mathbf{r},t) = \int d\mathbf{r}_1 \int_{-\infty}^{\infty} dt_1 V(\mathbf{r},\mathbf{r}_2) \otimes R(\mathbf{r}_2,\mathbf{r}_3,t,t_1) \otimes V(\mathbf{r}_3,\mathbf{r}_1)\rho^{\rm ext}(\mathbf{r}_1,t_1),$$

where $R(\mathbf{r},\mathbf{r}_1,t,t_1)$ is the retarded response function of the polarizable system, $V(\mathbf{r},\mathbf{r}')$ is the bare Coulomb interaction, and $\otimes$ denotes convolution in the coordinate $\mathbf{r}$, then Eq. (2) becomes

$$P(t) = \int d\mathbf{r} \int d\mathbf{r}_1 \int_{-\infty}^{\infty} dt_1 \rho^{\rm ext}(\mathbf{r},t)V(\mathbf{r},\mathbf{r}_2) \otimes \frac{d}{dt}R(\mathbf{r}_2,\mathbf{r}_3,t,t_1) \otimes V(\mathbf{r}_3,\mathbf{r}_1)\rho^{\rm ext}(\mathbf{r}_1,t_1). \tag{3}$$

The energy loss rate $P(t)$ in Eq. (3) contains both reactive (reversible) and dissipative (irreversible) losses. If the external charge is classical, the system cannot influence it, i.e., the system cannot give energy back to the external charge (which moves with uniform velocity without recoil). So the external charge loses energy to both channels. However, we will see that the situation is different if the external perturbation and response have quantum-mechanical character.

Our system will consist of two parallel metallic slabs separated by the distance D, with one of the slabs in the region $-L_1 \leqslant z \leqslant 0$ with electron density corresponding to r_{s1} and the other one in the region $D \leqslant z \leqslant d + L_2$ with electron density corresponding to r_{s2}. In other words, D is the distance between the points where the electron densities of the two slabs practically vanish, while the distance between jellium edges is $d = D + 2\Delta$ (Fig. 2), where Δ is the characteristic electron-density decay length. The jellium thicknesses are then $a_1 = L_1 - 2\Delta$ and $a_2 = L_2 - 2\Delta$.

Suppose that the left slab is moving parallel to the right one with relative velocity $\mathbf{v}$. In spite of charge neutrality and parallel translational invariance, there is still interaction between charge-density fluctuations because of their quantum-mechanical character, which also leads to the van der Waals force. For example, suppose that a charge-density fluctuation is spontaneously created in the left slab at the moment t_1 (Fig. 2). Propagating in time between t_1 and t it induces charge-density fluctuations in the right slab with which it can subsequently interact. In such a process, the left slab can be considered as a source that is transferring energy to the right slab and,

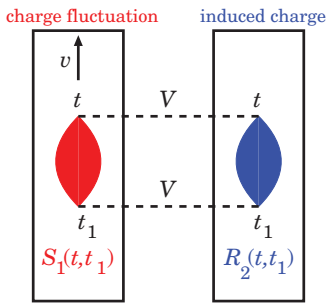

FIG. 2. (Color online) Process in which charge density fluctuation is created in the left slab and induces a potential in the right slab.

in analogy with Eq. (3), the energy loss rate operator can be written as

$$\hat{P}_{12} = \int d\mathbf{r} \int d\mathbf{r}_1 \int_{-\infty}^{\infty} dt_1 \hat{\rho}(\mathbf{r},t) V(\mathbf{r},\mathbf{r}_2) \otimes \frac{d}{dt} R_2(\mathbf{r}_2,\mathbf{r}_3,t,t_1) \otimes V(\mathbf{r}_3,\mathbf{r}_1)\hat{\rho}(\mathbf{r}_1,t_1), \quad (4)$$

where R_2 is the retarded response function of the right slab and $\hat{\rho}(\mathbf{r},t)$ and $\hat{\rho}(\mathbf{r},t)$ are density operators, which represent quantum-mechanical charge-density fluctuations created and annihilated at points $(\mathbf{r}_1,t_1)$ and $(\mathbf{r},t)$, respectively. The energy transfer rate from the left to the right slab can be obtained by taking the ground-state matrix element of Eq. (4),

$$P_{12} = \langle \hat{P}_{12}(t) \rangle = \int d\mathbf{r} \int d\mathbf{r}_1 \int_{-\infty}^{\infty} dt_1 S_1(\mathbf{r},\mathbf{r}_1,t,t_1) V(\mathbf{r},\mathbf{r}_2) \otimes \frac{d}{dt} R_2(\mathbf{r}_2,\mathbf{r}_3,t,t_1) \otimes V(\mathbf{r}_3,\mathbf{r}_1),$$

where

$$S_1(\mathbf{r},\mathbf{r}_1,t,t_1) = \langle \hat{\rho}(\mathbf{r},t)\hat{\rho}(\mathbf{r}_1,t_1) \rangle + \langle \hat{\rho}(\mathbf{r}_1,t_1)\hat{\rho}(\mathbf{r},t) \rangle \quad (5)$$

is the correlation function of the left slab, which represents real charge-density fluctuation. Equation (5) can be illustrated by the Feynman diagram in Fig. 2. We note that in the inertial system of the right slab the charge density in the left slab, apart from the fluctuations, has an additional parallel component of motion, so all parallel coordinates in the left slab have to be transformed as

$$\boldsymbol{\rho} \to \boldsymbol{\rho} - \mathbf{v}t. \quad (6)$$

Explicitly, the correlation function (5) becomes

$$S_1(\mathbf{r},\mathbf{r}_1,t,t_1) = S_1(z,z_1,\boldsymbol{\rho} - \mathbf{v}t, \boldsymbol{\rho}_1 - \mathbf{v}t_1,t,t_1). \quad (7)$$

After inserting Eq. (7) into Eq. (5) and Fourier transformation in parallel coordinates and time, we get the formula for energy transfer rate per unit surface from the left to the right slab:

$$P_{12} = -i\hbar \int_{-\infty}^{\infty} dz \int_{-\infty}^{\infty} dz_1 \int \frac{d\mathbf{Q}}{(2\pi)^2} \int_{-\infty}^{\infty} \frac{d\omega}{2\pi} \times (\omega + \mathbf{Q}\cdot\mathbf{v}) S_1(\mathbf{Q},|\omega|,z,z_1) V(\mathbf{Q},z,z_2) \otimes R_2(\mathbf{Q},\omega+\mathbf{Q}\cdot\mathbf{v},z_2,z_3) \otimes V(\mathbf{Q},z_3,z_1). \quad (8)$$

If we use

$$V(\mathbf{Q},z,z_2) = v_Q e^{-Q(z_2-z)},$$
$$V(\mathbf{Q},z_3,z_1) = v_Q e^{-Q(z_3-z_1)},$$

the definition of the surface excitation propagator[24]

$$D(\mathbf{Q},\omega) = v_Q \int dz_1 dz_2 e^{Qz_1} R(\mathbf{Q},\omega,z_1,z_2) e^{Qz_2}, \quad (9)$$

and the definition of the surface correlation function

$$S(\mathbf{Q},\omega) = v_Q \int dz_1 dz_2 e^{Qz_1} S(\mathbf{Q},\omega,z_1,z_2) e^{Qz_2}, \quad (10)$$

Eq. (8) can be written as

$$P_{12} = -i\hbar \int \frac{d\mathbf{Q}}{(2\pi)^2} \int_{-\infty}^{\infty} \frac{d\omega}{2\pi} e^{-2Qd} S_1(\mathbf{Q},|\omega|) \times \omega + \mathbf{Q}\cdot\mathbf{v} D_2(\mathbf{Q},\omega+\mathbf{Q}\cdot\mathbf{v}). \quad (11)$$

Using the connection between the surface correlation function and the imaginary part of the surface excitation propagator,

$$\mathrm{Im}D_1(\mathbf{Q},\omega) = \mathrm{sgn}\omega S_1(\mathbf{Q},|\omega|), \quad (12)$$

Eq. (11) can be written as

$$P_{12} = -i\hbar \int \frac{d\mathbf{Q}}{(2\pi)^2} \int_{-\infty}^{\infty} \frac{d\omega}{2\pi} e^{-2Qd} (\omega + \mathbf{Q}\cdot\mathbf{v})\mathrm{sgn}\omega \times \mathrm{Im}D_1(\mathbf{Q},\omega) D_2(\mathbf{Q},\omega+\mathbf{Q}\cdot\mathbf{v}). \quad (13)$$

Finally, as the imaginary part of surface excitation propagator (12) is an odd function of frequency, P_{12} given by Eq. (13) is a real quantity,

$$P_{12} = \hbar \int \frac{d\mathbf{Q}}{(2\pi)^2} e^{-2Qd} \int_{-\infty}^{\infty} \frac{d\omega}{2\pi} (\omega + \mathbf{Q}\cdot\mathbf{v})\mathrm{sgn}\omega \times \mathrm{Im}D_1(\mathbf{Q},\omega)\mathrm{Im}D_2(\mathbf{Q},\omega+\mathbf{Q}\cdot\mathbf{v}). \quad (14)$$

The Feynman diagram which illustrates Eq. (14) is shown in Fig. 3(a). We see that if the charge fluctuation is created with the energy ω, it can create excitations in the right slab with the energy $\omega + \mathbf{v}\cdot\mathbf{Q}$. This is expected, namely, ω is the energy in the inertial system of the left slab but, in the inertial system of the right slab, it is Doppler shifted by $\mathbf{v}\cdot\mathbf{Q}$. We see that even when $\mathbf{v} = 0$ the energy transfer rate is finite $P_{12} \neq 0$, which is a correct result. Namely, P_{12} describes how much energy is transferred from the left to the right slab, but we still do

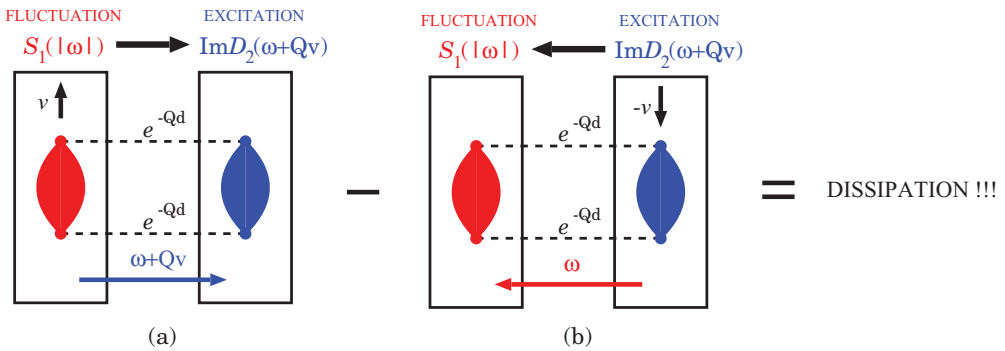

FIG. 3. (Color online) Process in which the energy $\omega + \mathbf{v}\cdot\mathbf{Q}$ is transferred from the left to the right slab (a), and the reverse process in which energy ω is returned back to the left slab (b).

not know how much of this energy is transferred irreversibly. For example, if the charge fluctuation in the left slab were classical (some external time-dependent charge), then all the energy P_{12} given by Eq. (14) would be irreversibly transferred (dissipated) to the right slab. However, the charge fluctuations in right slab are quantum mechanical and all work done by that charge could be reversibly recovered.

In order to find the reversible work done by the charge fluctuation in the left slab, i.e., the energy which is only "borrowed"to the right slab, we have to work in the inertial system of the left slab, i.e., repeat the same calculation but with the response functions of the right slab transformed as

$$R_2(\mathbf{r},\mathbf{r}_1,t,t_1) = R_2(z,z_1,\boldsymbol{\rho}+\mathbf{v}t,\boldsymbol{\rho}_1+\mathbf{v}t_1,t,t_1) \qquad (15)$$

and the coordinates of the correlation function in the left slab remaining unchanged. Inserting Eq. (15) into Eq. (5) and repeating the same calculation, we obtain

$$P'_{12} = \hbar\int\frac{d\mathbf{Q}}{(2\pi)^2}e^{-2Qd}\int_{-\infty}^{\infty}\frac{d\omega}{2\pi}\,\omega\,\mathrm{sgn}\omega \times \mathrm{Im}D_1(\mathbf{Q},\omega)\mathrm{Im}D_2(\mathbf{Q},\omega+\mathbf{Q}\cdot\mathbf{v}). \qquad (16)$$

Expression (16) represents the amount of energy that is transferred from the left to right but that will be reversibly returned back, as shown in Fig. 3(b). Therefore, the amount of energy that is irreversibly transferred from left to right (dissipated energy) is

$$P_1^{\mathrm{diss}} = P_{12} - P'_{12} = \hbar\mathbf{v}\int\frac{d\mathbf{Q}}{(2\pi)^2}\,\mathbf{Q}\,e^{-2Qd}\int_{-\infty}^{\infty}\frac{d\omega}{2\pi}\mathrm{sgn}\omega \times \mathrm{Im}D_1(\mathbf{Q},\omega)\mathrm{Im}D_2(\mathbf{Q},\omega+\mathbf{v}\cdot\mathbf{Q}). \qquad (17)$$

We have to notice that the charge degrees of freedom in the left slab can be divided into quantum mechanical (fluctuations in the inertial system of the left slab) and classical (relative motion with velocity $\mathbf{v}$). Exactly that classical motion prevents the energy from being fully restored.

Similarly, energy can be dissipated due to the process where the charge fluctuation in the right slab induces the fluctuations in the left slab. The corresponding dissipation energy rate can be obtained from Eq. (17) by exchanging 1 and 2 and replacing $\mathbf{v}$ by $-\mathbf{v}$,

$$P_2^{\mathrm{diss}} = -\hbar\mathbf{v}\int\frac{d\mathbf{Q}}{(2\pi)^2}\mathbf{Q}\,e^{-2Qd}\int_{-\infty}^{\infty}\frac{d\omega}{2\pi} \times \mathrm{sgn}(\omega)\mathrm{Im}D_1(\mathbf{Q},\omega-\mathbf{v}\cdot\mathbf{Q})\mathrm{Im}D_2(\mathbf{Q},\omega). \qquad (18)$$

After changing the variable of integration $\mathbf{Q}\to-\mathbf{Q}$ in Eq. (18), the total dissipation energy rate can be written as

$$P = P_1^{\mathrm{diss}} + P_2^{\mathrm{diss}} = \hbar\mathbf{v}\int\frac{d\mathbf{Q}}{(2\pi)^2}\mathbf{Q}\,e^{-2Qd}\int_{-\infty}^{\infty}\frac{d\omega}{2\pi}\mathrm{sgn}(\omega) \times [\mathrm{Im}D_1(\mathbf{Q},\omega)\mathrm{Im}D_2(\mathbf{Q},\omega+\mathbf{v}\cdot\mathbf{Q}) + \mathrm{Im}D_1(\mathbf{Q},\omega+\mathbf{v}\cdot\mathbf{Q})\mathrm{Im}D_2(\mathbf{Q},\omega)]. \qquad (19)$$

In the symmetrical case, $D_1 = D_2$ and Eq. (19) can be simplified:

$$P = 2\hbar\mathbf{v}\int\frac{d\mathbf{Q}}{(2\pi)^2}\mathbf{Q}\,e^{-2Qd}\int_{-\infty}^{\infty}\frac{d\omega}{2\pi}\mathrm{sgn}(\omega) \times \mathrm{Im}D(\mathbf{Q},\omega)\mathrm{Im}D(\mathbf{Q},\omega+\mathbf{v}\cdot\mathbf{Q}). \qquad (20)$$

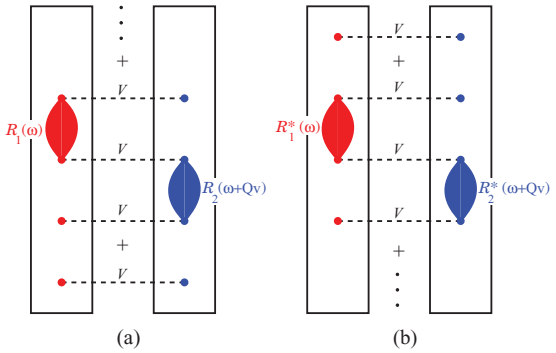

FIG. 4. (Color online) Higher-order processes.

All higher-order processes can be included very simply. The bare Coulomb interaction in Figs. 2(a) and 2(b) has to be replaced by the screened Coulomb interaction, as shown in Figs. 4(a) and 4(b). In (Q,ω) space, it corresponds to replacing the vertex which appears in D_1,

$$v_Q \;\to\; v_Q(1+D_2D_1e^{-2Qd}+\cdots) = \frac{v_Q}{1-D_2D_1e^{-2Qd}},$$

and the one which appears in D_2,

$$v_Q \;\to\; v_Q(1+D_1^*D_2^*e^{-2Qd}+\cdots) = \frac{v_Q}{1-D_1^*D_2^*e^{-2Qd}}.$$

So the final expression for the dissipated energy becomes

$$P = \mathbf{v}\int\frac{d\mathbf{Q}}{(2\pi)^2}\mathbf{Q}\,e^{-2Qd}\int_{-\infty}^{\infty}\frac{d\omega}{2\pi}\mathrm{sgn}(\omega) \times\left[\frac{\mathrm{Im}D_1(\mathbf{Q},\omega)\mathrm{Im}D_2(\mathbf{Q},\omega+\mathbf{v}\cdot\mathbf{Q})}{|1-D_2(\mathbf{Q},\omega+\mathbf{v}\cdot\mathbf{Q})D_1(\mathbf{Q},\omega)e^{-2Qd}|^2} + \frac{\mathrm{Im}D_1(\mathbf{Q},\omega+\mathbf{v}\cdot\mathbf{Q})\mathrm{Im}D_2(\mathbf{Q},\omega)}{|1-D_1(\mathbf{Q},\omega+\mathbf{v}\cdot\mathbf{Q})D_2(\mathbf{Q},\omega)e^{-2Qd}|^2}\right]$$

or, for the symmetrical case,

$$P = 2\hbar\mathbf{v}\int\frac{d\mathbf{Q}}{(2\pi)^2}\mathbf{Q}\,e^{-2Qd}\int_{-\infty}^{\infty}\frac{d\omega}{2\pi}\mathrm{sgn}(\omega) \times\frac{\mathrm{Im}D(\mathbf{Q},\omega)\mathrm{Im}D(\mathbf{Q},\omega+\mathbf{v}\cdot\mathbf{Q})}{|1-D(\mathbf{Q},\omega)D(\mathbf{Q},\omega+\mathbf{v}\cdot\mathbf{Q})e^{-2Qd}|^2}. \qquad (21)$$

When $\mathbf{v}\neq0$, the dissipated energy rate is $P\neq0$, so if one wants to maintain a constant velocity $\mathbf{v}$ of the left slab, one has to do the work that is equal and opposite to the dissipated energy (21), i.e.,

$$P = -\mathbf{F}\cdot\mathbf{v}. \qquad (22)$$

After combining Eqs. (22) and (21), we get the formula for the frictional force:

$$\mathbf{F} = -2\hbar\int\frac{d\mathbf{Q}}{(2\pi)^2}\mathbf{Q}\,e^{-2Qd}\int_{-\infty}^{\infty}\frac{d\omega}{2\pi}\mathrm{sgn}(\omega) \times\frac{\mathrm{Im}D(\mathbf{Q},\omega)\mathrm{Im}D(\mathbf{Q},\omega+\mathbf{v}\cdot\mathbf{Q})}{|1-D(\mathbf{Q},\omega)D(\mathbf{Q},\omega+\mathbf{v}\cdot\mathbf{Q})e^{-2Qd}|^2}. \qquad (23)$$

If we suppose that $\mathbf{v} = v\mathbf{x}$, then Eq. (23) can also be written as[14]

$$F_x = \frac{\hbar}{\pi^3}\int_0^\infty Q_x dQ_x \int_0^\infty dQ_y e^{-2Qd}\int_0^{vQ_x} d\omega \times \frac{\mathrm{Im}D(\mathbf{Q},\omega)\mathrm{Im}D(\mathbf{Q},\omega - vQ_x)}{|1 - D(\mathbf{Q},\omega)D(\mathbf{Q},\omega - vQ_x)e^{-2Qd}|^2}. \quad (24)$$

III. NONLOCALITY, DISPERSION, AND DISSIPATION

We observe that expressions (19)–(24) are formally identical to those obtained by Pendry[14] and Persson[15] and, in fact, up to this point this is expected. The most important input in the expressions for the friction (as well as van der Waals and Casimir energies) are the values of the EM fields in the region between surfaces located at $z = 0$ and $z = d$, and these values can be completely defined by reflectivities $D_i(\mathbf{Q},\omega)$, where $i = 1,2$. While these reflectivities in principle could contain everything, including nonlocal effects, other (nonelectronic) excitation mechanisms, etc., the main theoretical problem becomes how to determine them to describe adequately the screening properties of the electrons in the two slabs.

Therefore, before proceeding further, we shall comment on the problem of nonlocality, with specific reference to finite systems. In the infinite homogenous solid, one can describe dielectric properties by means of a frequency and three-dimensional (3D) momentum dependent response function $R(\mathbf{q},\omega)$ and the related dielectric function $\epsilon(\mathbf{q},\omega)$. These quantities are "nonlocal," i.e., they spatially depend on the relative distance as $R(\mathbf{r} - \mathbf{r},\omega)$ and $\epsilon(\mathbf{r} - \mathbf{r},\omega)$, respectively. Therefore, one can describe EM fields at each point by means of the transverse and longitudinal dielectric functions. In a finite system, an additional nonlocality appears due to the breakdown of translational symmetry. For example, in the system with planar symmetry, the response function $R(\boldsymbol{\rho} - \boldsymbol{\rho}',z,z',\omega)$ is not a function of the relative distance $z - z'$, so its Fourier transform $R(\mathbf{Q},q,q',\omega)$ depends on the parallel wave vector $\mathbf{Q}$, but is nondiagonal in its perpendicular components. The dielectric function also can be written as a matrix $\epsilon(\mathbf{Q},q,q',\omega)$(see, e.g., Ref. 25), but its use in the description of the EM fields becomes difficult. All attempts to simplify these expressions, e.g., neglecting nondiagonal ($q \neq q'$) terms in R and ϵ, lead to new difficulties, which require additional boundary conditions, etc. Usual Fresnel equations describing reflection and transmission of EM waves in finite systems were developed in the classical electrodynamics for a local case, i.e., medium (or media) defined by a spatially (i.e., momentum) independent dielectric function (or functions), separated by sharp boundaries. Therefore, the inclusion of nonlocality and smooth electron-density profiles at surfaces presents a difficult problem, especially if one insists on the use of the dielectric function. Therefore, in the so-called nonlocal optics, one usually applies the Fresnel formulas, e.g., for reflectivity, assuming sharp boundaries, and describes nonlocality by adding some wave vector dependence in the dielectric function, neglecting its tensorial character. This modification can be provided, e.g., by the hydrodynamical model or the semiclassical infinite barrier model, etc. Needless to say, this procedure requires approximations that sometimes cannnot be justified. In this paper, as in the previous work on van der Waals[24] and Casimir forces,[26] we have avoided such difficulties and particularly the use of the dielectric function (or tensor). Our results (19)–(24) are derived using a field-theoretical method that does not involve explicitly the knowledge of electromagnetic fields or their matching at surfaces. They involve generalized reflectivities $D(\mathbf{Q},\omega)$ that describe dynamical nonlocal response of each metallic slab. We have already shown[24,26] that generalized reflectivities correctly reduce to the local expressions based on the dielectric functions in the long-wavelength limit.[14,23] Our response functions are calculated using wave functions obtained in the Density Functional-Local Density Approximation (DF-LDA) approach and, with the same wave functions, we reproduce smooth charge-density profiles at the surfaces. Also, through a self-consistent LDA approach, exchange and local correlations were included in these wave functions, which means that our procedure goes beyond random-phase approximation (RPA).

IV. COMPARISON WITH THE LOCAL MODELS

As mentioned in the Introduction, we want to discuss the effects of nonlocality, i.e., spatial dispersion of electronic excitations in finite systems, but not the dissipation, even if it is present in real systems. Our calculation therefore does not include any dissipation: it is even incorrect to describe a very important process—excitation of electron-hole pairs as "Landau damping." (Of course, one should not confuse these dissipation mechanisms with the energy dissipation that is the essence of the friction process.)

In this section, we shall therefore compare our results for the friction force (for the symmetrical case) with two local models for the reflectivity $D(\mathbf{Q},\omega)$ in order to analyze nonlocal effects only, first neglecting and later including dissipation. As we do not want to discuss the effects of other scattering mechanisms, which certainly contribute to friction â phonons, impurities, etc. (and which can anyway be described in the Drude model only approximately), the real measure of our nonlocality can be the comparison with the Drude model without dissipation (which is in fact equivalent to the plasmon model). We shall add the comparison with the Drude model with dissipation only to emphasize inadequacy of all local models to describe low velocity friction, even when dissipation is included.

In the local models, the surface plasmon propagator for a semi-infinite solid is given by

$$D_l^S[\epsilon(\omega)] = \frac{\epsilon(\omega) - 1}{\epsilon(\omega) + 1}, \quad (25)$$

where $\epsilon(\omega)$ is the local dielectric function, so that D_l does not explicitly depend on Q. For the slab of thickness a, we have to replace

$$D_l^S[\epsilon(\omega)] \to D_l^F[Q,\epsilon(\omega)] = D_l^S[\epsilon(\omega)]\frac{1 - e^{-2Qa}}{1 - \left\{D_l^S[\epsilon(\omega)]\right\}^2 e^{-2Qa}}. \quad (26)$$

We shall apply Eqs. (25) and (26) to the (dispersionless) plasmon model, where

$$\epsilon_p(\omega) = 1 - \frac{\omega_p^2}{\omega^2} \quad (27)$$

and ω_p is the plasma frequency. In the plasmon model, the surface spectral function is obtained as

$$S_p(Q,\omega) = \mathrm{Im} D_l^F[Q,\epsilon_p(\omega + i\eta)], \tag{28}$$

where η is infinitesimally small. In the Drude model, the local dielectric function is obtained from the dielectric function (27) as

$$\epsilon_D(\omega,\delta) = 1 - \frac{\omega_p^2}{\omega(\omega + i\delta)},$$

where δ is a phenomenological parameter describing dissipation in the system in terms of the plasmon damping. The surface spectral function is then

$$S_D(Q,\omega) = \mathrm{Im} D_l^F[Q,\epsilon_D(\omega,\delta)]. \tag{29}$$

For the proper nonlocal description, we shall use our numerically calculated results for $D(Q,\omega)$ in Refs. 25, 27, and 28. We first construct the noninteracting response function,

$$R^0(\mathbf{Q},\omega,z,z') = \sum_{n,m,\mathbf{K}} \frac{f(E_{n,\mathbf{K}}) - f(E_{m,\mathbf{K}+\mathbf{Q}})}{\omega - (E_{m,\mathbf{K}+\mathbf{Q}} - E_{n,\mathbf{K}}) + i\eta} \times \Phi_n(z)\Phi_m(z)\Phi_n(z')\Phi_m(z'), \tag{30}$$

where $\Phi_n(z)$ and $E_{n,\mathbf{K}} = \frac{\hbar^2 K^2}{2m} + E_n$ are the Kohn-Sham wave functions and energies in a metallic slab, and

$$f(E_{n,\mathbf{K}}) = \theta(E_F - E_{n,\mathbf{K}})$$

is the Fermi-Dirac distribution function for $T = 0$. By inserting Eq. (30) into the RPA-Dyson equation

$$R(\mathbf{Q},\omega,z,z') = R^0(\mathbf{Q},\omega,z,z') + \int_{-L}^{0} dz_1 \int_{-L}^{0} dz_2 R^0(\mathbf{Q},\omega,z,z_1) \times V(\mathbf{Q},z_1,z_2) R(\mathbf{Q},\omega,z_2,z'), \tag{31}$$

we obtain the screened response function $R(\mathbf{Q},\omega,z,z')$, which then can be inserted into the formula for the surface excitation propagator, Eq. (9). The surface spectral function,

$$S(\mathbf{Q},\omega) = \mathrm{Im} D(\mathbf{Q},\omega), \tag{32}$$

calculated from Eqs. (10) and (31) is shown in Fig. 5 (red solid line) for a set of parameters.

The shapes of these spectra are very instructive and can explain nonlocal modifications of the friction because they correspond to surface reflectivities in Eq. (24). In the Drude model, we see two (for a finite slab) slightly broadened surface plasmon peaks (black dotted lines), but nonlocal calculations (red solid lines) contain a number of low-energy structures arising from single-particle (intra- and interband) electron-hole transitions. The discrepancy between these two calculations is most obvious in the low-energy region. Even the structures at the surface plasmon frequencies differ from simple resonance shapes.

A. Calculations without dissipation

To obtain some general feeling about the force-velocity scales, we shall first calculate the friction force for the simplest case, i.e., two semiinfinite metals treated in a plasmon model

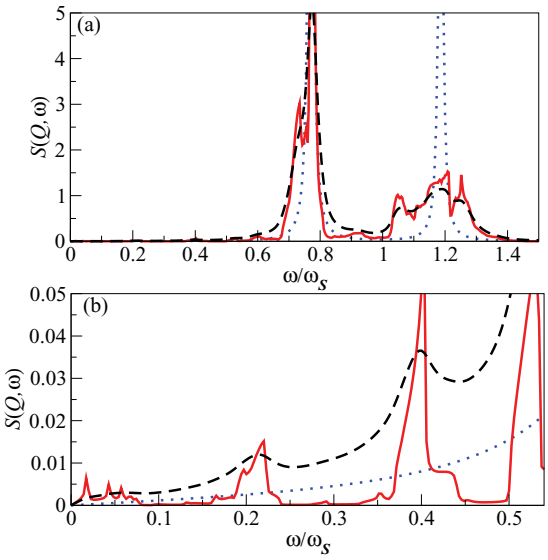

FIG. 5. (Color online) (a) Spectrum of electronic excitations in silver film for $Q = 0.029 a_0^{-1}$. Nonlocal result without dissipation (red solid line), nonlocal result with dissipation for $\eta = 100$ meV (black dashed line), and Drude model for $\eta = 100$ meV (blue dotted line). (b) Same as in (a), but in the lower-frequency interval. Slab thickness is $31 a_0$ and $r_s = 3$.

up to very large velocities, using the expression for the surface spectral function,

$$\mathrm{Im} D(\mathbf{Q},\omega) = \frac{\pi \omega_S}{2} [\delta(\omega - \omega_S) - \delta(\omega + \omega_S)],$$

where $\omega_S = \frac{\omega_p}{\sqrt{2}}$ is the surface plasmon frequency. As expected, we obtain Pendry's result[19] for the friction force derived in the lowest order:

$$F_x(d,v) = \frac{\hbar \omega_S^3}{2\pi v^2} \int_0^\infty dQ_y e^{-2d\sqrt{(\frac{2\omega_S}{v})^2 + Q_y^2}}, \tag{33}$$

which can be also integrated to give

$$F_x(d,v) = \frac{2\hbar\omega_S^4}{\pi v^3} K_1\left(4d\frac{\omega_S}{v}\right), \tag{34}$$

where K_1 is the modified Bessel function.

The force (34) for two semi-infinite metals at the distance $d = 24 a_0$ and for $r_s = 3$ is shown in Fig. 6. The velocity is given in m/s, the Fermi velocity corresponding to $r_s = 3$ is $v_F = 1.4 \times 10^6$ m/s, $\hbar\omega_p = 9.1$ eV, and $\hbar\omega_S = 6.4$ eV.

The condition for the excitation process is $Q_x v = 2\omega_S$, so for low velocities obviously only very large Q plasmons can be excited, and the friction force approaches zero as $v^{-5/2} e^{-a}$, where $a = \frac{4\omega_S d}{v}$. For larger velocities ($v \approx 10^7$ m/s), friction is increasing very fast, because low Q plasmons start to contribute. The force reaches its maximum at $v = 2.07 \times 10^7$ m/s [or $v = 0.84\ (\frac{1}{2\omega_S d})$] and after that slowly decreases as $1/v^2$, but all this occurs at unphysically high velocities. It is obvious that the physically relevant is only the region of low velocities $v << 4\omega_S d$.

Therefore, in Fig. 7, we present the friction between two metallic slabs of thicknesses $L = 31 a_0$ and $r_s = 3.0$ at lower velocities, calculated in three different models: plasmon, Drude, and the full nonlocal theory.

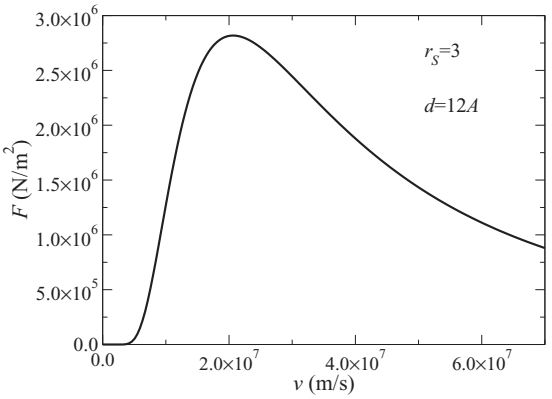

FIG. 6. Friction force between two semi-infinite metals in the plasmon model. Separation between surfaces is $d = 24a_0$ and $r_s = 3$, corresponding to $\hbar\omega_S = 6.4$ eV.

In Fig. 7(a) (inset), we see that for large velocities the nonlocal result (red dotted line) approaches the plasmon model result (black solid line). This is to be expected, because for very high velocities energy can be dissipated only by exciting low Q eigenmodes, i.e., surface plasmons, which then dominate the spectra, while the electron-hole pair continuum has a negligible spectral weight.

For lower and more realistic velocities the situation is quite different and, as one can see from Fig. 7(a), friction force is one order of magnitude stronger than in the plasmon model, where only large Q plasmons that have a small spectral weight can be excited. However, nonlocal calculation includes a continuum of low Q,ω electron-hole excitations, which can be excited and become the dominant dissipation channel, while plasmon excitation gives a negligible contribution to friction.

B. Calculations with dissipation

In order to investigate how well the Drude model, with its phenomenologically introduced dissipation, could describe the friction in the region where we observe electron-hole excitations in the nonlocal theory, in Fig. 7(a) we also present results in this model (blue dashed line).

The Drude model does not qualitatively differ from the plasmon model result even for unreasonably large damping constant. This means that for smaller velocities ($v < 3 \times 10^6$ m/s) friction force exists only because of energy dissipation into low-energy electron-hole excitations.

In Fig. 7(b), we present results for friction force for a larger slab separation ($d = 100a_0$). The range of the excitation momenta Q involved in the process is now shifted to lower $Q \approx \frac{1}{d}$, which strongly reduces friction force. The difference between plasmon and RPA-LDA nonlocal calculations qualitatively remains unchanged, but we see that now Drude damping contributes substantially to friction. The reason is that only low-(Q,ω) modes can be excited (in a large velocity interval) and here dissipation arises from the large low-energy tail of the Drude damped plasmon (as shown in Fig. 5). So in a certain velocity interval, and for larger separations, Drude damping can simulate the effect of the low-energy electron-hole continuum, as we shall discuss in Sec. IV C. Still (as we will see later), for lower velocities ($v < 10^6$ m/s) the Drude model is no longer able to reproduce nonlocal results. When the damping constant δ is reduced, the Drude result approaches the plasmon model, as expected.

Until now we have compared the results of the Drude model with nonlocal results calculated without dissipation. We shall next include some decay mechanisms in the calculation of the electronic response in order to compare the two models under similar and more realistic conditions, i.e., by including some dissipative processes.

Before proceeding, it is important to first distinguish between processes that are considered as "dissipation" and those that contribute to friction. The friction force between metallic slabs can be understood as a loss of kinetic energy to excitations of various modes inside the slabs. Within the framework of the model used here, only collective and

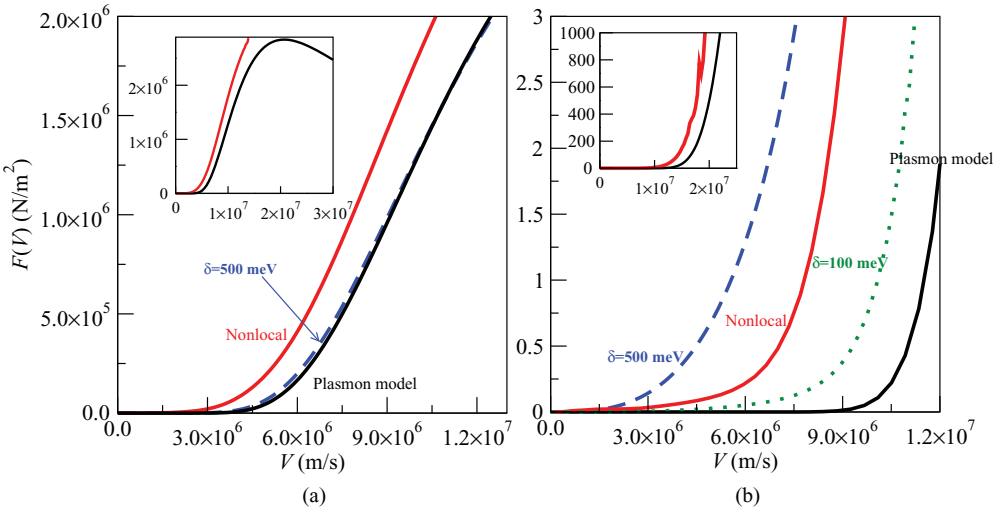

FIG. 7. (Color online) Friction force between two metallic slabs at distance (a) $d = 24a_0$ and (b) $d = 100a_0$ in the plasmon model (black solid line), Drude model for $\delta = 100$ meV (red dotted line), Drude model for $\delta = 500$ meV (blue dashed line), and nonlocal calculations in the jellium model (solid red line). Inserted pictures show nonlocal and plasmon model results for the friction force at larger velocities. Slab thickness is $a = 31a_0$ and $r_s = 3$.

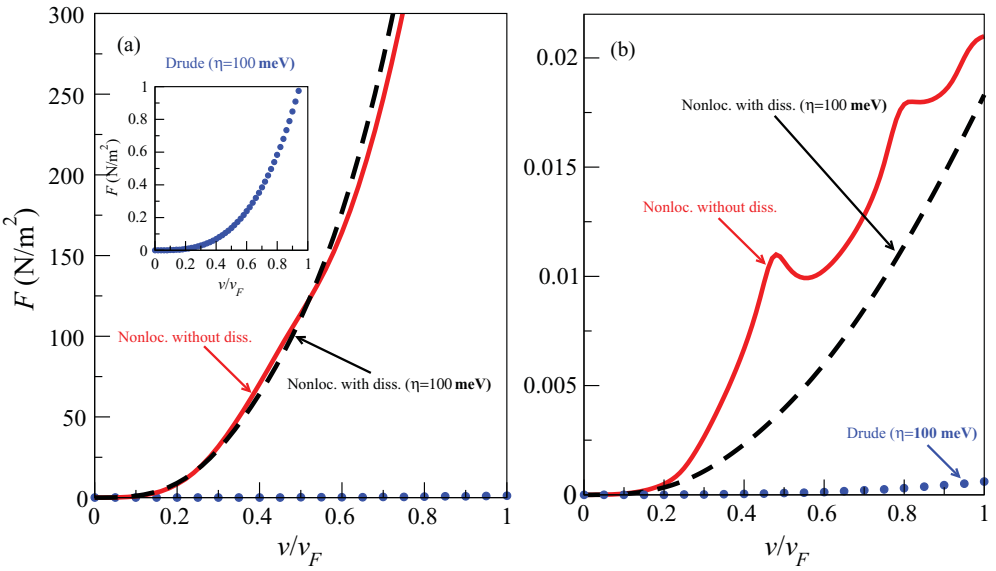

FIG. 8. (Color online) Friction force between two metallic films at distance (a) $d = 24a_0$ and (b) $d = 100a_0$. Nonlocal calculation without dissipation (red solid line), nonlocal calculation with dissipation for $\delta = 100$ meV (black dashed line), and Drude calculation for $\eta = 100$ meV (blue dotted line). Slab thickness is $a = 31a_0$ and $r_s = 3$. Inserted picture shows Drude result at small separation $d = 24a_0$.

single-particle electronic excitations contribute to friction. Both types of modes consist of many electron-hole excitations. The system without dissipation is defined as a system in which electrons and holes do not decay once created, i.e., between creation and annihilation their motion is collisionless. For a real metal, electrons and holes can decay due to collisions (mediated by the Coulomb interaction) or excitations of phonons, scattering on impurities, dislocations, etc. This provides broadening to the electron and hole spectra.

The simplest way to describe this decay mechanism for electronic states is by including a finite imaginary part, corresponding to a relaxation frequency, in the denominator of the response function (30). In Fig. 5, we show the spectra of electronic excitations calculated with the damping parameter $\eta = 100$ meV (black dashed lines), as we have used in the Drude model. The spectra are smoother, but their weight distribution is not modified with respect to the $\eta \to 0^+$ limit.

In Fig. 8, we show the low velocity friction calculated in the nonlocal model with and without dissipation for two separations, and see that they show the same magnitude and overall behavior. This result, as well as the negligible friction in the Drude model, can be easily explained by inspection of the frequency dependence of the imaginary part of reflectivities in Fig. 5. The main contribution to friction, as explained earlier, comes from electron-hole pairs (low-energy oscillations in the inset in Fig. 5), irrespective of their dissipation, and the Drude (as well as plasmon) model cannot describe friction for $v \leqslant v_F$. The only difference between nonlocal results with and without dissipation for $d = 25a_0$ are weak oscillations, which only appear in the nondissipative case. These oscillations are due to intraband electron-hole excitations within 2D bands, which are the consequence of the quantization of the electronic states along z direction. When dissipation is included, these weak oscillations are smoothed out, as shown in Fig. 8(a).

At larger distance $d = 100a_0$, lower Q values dominate, and in Fig. 8(b) we observe stronger oscillations appearing at the thresholds for electronic 2D intraband transitions. Inclusion of dissipation indeed modifies, i.e., suppresses, these oscillations, and also somewhat reduces friction, which however approaches the same value for large velocities. For both distances, the local (Drude model for $\eta = 100$ meV) contribution to friction is shown to be negligible as compared to the nonlocal one.

C. Drude model at large separations

In Sec. IV B, we mentioned that at large separations the tail of the Drude plasmon could give a similar contribution to friction as the low-energy electron-hole continuum. Now we shall show that this is only an accidental agreement which has no physical significance.

For velocities of physical interest $v \leqslant v_F$ (typical group velocity of electrons in metals), we can find an approximate analytic expression for the friction force dependence, taking the lowest-order term in Eq. (24) and using the asymptotic form of $S(\mathbf{Q},\omega)$ (for a semi-infinite metal) for low momenta ($Q \ll k_F$) and frequencies ($\omega \ll \omega_p$),[15] which includes electron-hole excitations:

$$S(\mathbf{Q},\omega) = 2\zeta(Q)\,\frac{\omega}{\omega_p}\,\frac{Q}{k_F}, \tag{35}$$

where the function $\zeta(Q) \approx 1$ for $Q \to 0$. The frequency integration in Eq. (24) then gives $\frac{2}{3}\frac{Q^2 Q_x^3 v^3}{\omega_p^2 k_F^2}$ and the friction can be evaluated as

$$F_x = \alpha \left(\frac{v}{v_F}\right)^3, \tag{36}$$

where

$$\alpha = \frac{\hbar^6}{2\pi^2 e^2 m^4 d^8 v_F^2}\, I$$

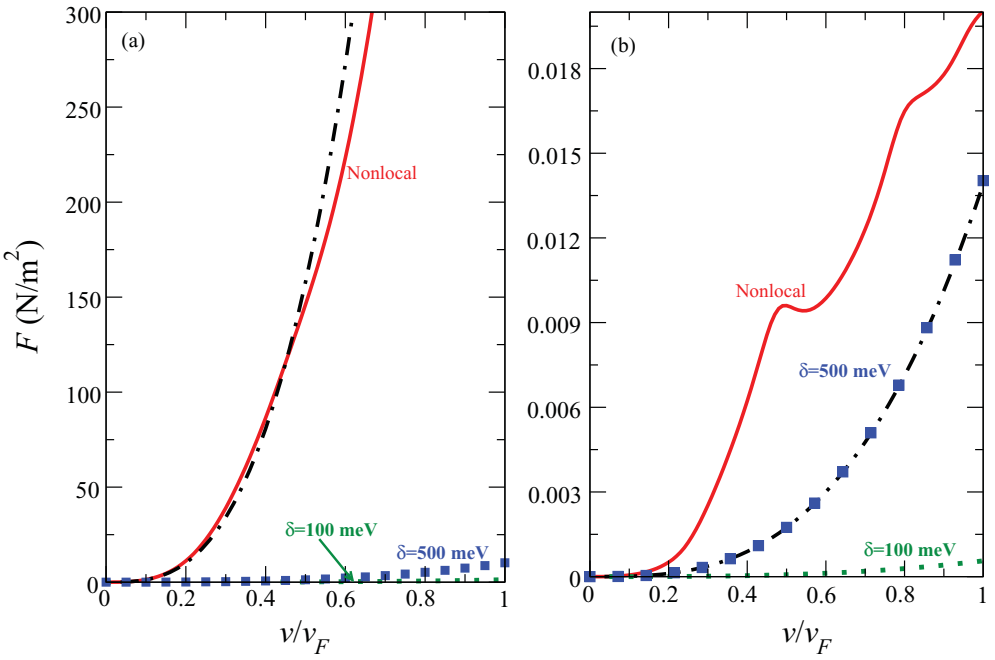

FIG. 9. (Color online) Friction force between two metallic films at distance (a) $d = 24a_0$ and (b) $d = 100a_0$ in the Drude model for $\delta = 100$ meV (green dotted line), for $\delta = 500$ meV (blue squares), and the nonlocal calculation in the jellium model (solid red line). Black dashed-dotted line represents the curve $\alpha\,(\frac{v}{v_F})^3$, where (a) $\alpha = 1262\,\mathrm{N/m^2}$ and (b) $\alpha = 0.0139\,\mathrm{N/m^2}$. Result for the plasmon model is not presented because it is negligible. Slab thickness is $a = 31a_0$ and $r_s = 3$.

and $I = 11.6$ is the value of the integral

$$I = \int_0^\infty dx\, x^4 \int_0^\infty dy (x^2 + y^2) e^{-2\sqrt{x^2+y^2}}.$$

We find that at $T = 0$ quantum friction increases as v^3, as shown before,[14] and decreases very fast with distance as $\frac{1}{d^8}$, which differs from Pendry's results, Eqs. (57) and (58) in Ref. 14, because he assumed a strictly local response. In Fig. 9, we shall show the friction for still lower velocities, which further confirm this result (36). For $d = 24a_0$, Eq. (36) gives $\alpha = 1262\,\mathrm{N/m^2}$, and the corresponding curve [dashed-dotted line in Fig. 9(a)] agrees very well with the calculated (nonlocal) friction [solid line in Fig. 9(a)]. For $d = 100a_0$, friction force is strongly reduced, but the agreement between the asymptotic expression (36), with $\alpha = 0.0139\,\mathrm{N/m^2}$, and the full nonlocal calculation is much worse than for smaller separations, as shown in Fig. 9(b). The reason is that friction at large separations d is dominated by small Q contributions, and here size quantization of electrons in the slab becomes important. In other words, the onset of interband transitions, not included in the expression (35), leads to the increase and oscillations in the nonlocal result, as shown in Fig. 9(b).

The low-energy spectral weight in the Drude model is weak and structureless [blue dotted line in Fig. 5(b)] and the corresponding force is very much reduced [blue dashed line in Fig. 9(a)]. Friction force in the plasmon model on this scale is negligible. However, it is interesting to note that the Drude result for a carefully chosen damping parameter can be made to agree with the asymptotic result (36). For example, in Fig. 9(b), the Drude result for $\delta = 500$ meV (blue squares) and the asymptotic result (black dash-dotted line) are almost identical. The reason is that the Drude spectrum [blue-dashed line in the inset of Fig. 9(a)] and the asymptotic spectrum (35) are both structureless and linear in ω for small ω. In fact, in the Drude model for small ω,

$$S_D(Q,\omega) \approx \frac{2\delta}{\omega_p^2}\,\omega, \tag{37}$$

and we can calculate the friction using the lowest-order term in Eq. (24) to find

$$F_x^D = \beta \left(\frac{v}{v_F}\right)^3, \tag{38}$$

where

$$\beta = \frac{3}{8\pi}\,\frac{\hbar^7\delta^2}{m^4e^4v_F^3d^6}\,J$$

and $J = 1.1$ is the value of the integral

$$J = \int_0^\infty dx\, x^4 \int_0^\infty dy\, e^{-2\sqrt{x^2+y^2}}.$$

Again we find the v^3 dependence of the friction, but now it depends on the distance as $1/d^6$, which is in agreement with Pendry' s result[14] derived using the local response. It turns out that the striking agreement between the asymptotic nonlocal and Drude results is achieved only if $\alpha = \beta$, which implies a specific value of the damping constant

$$\delta_C = \frac{1}{d}\sqrt{\frac{4Ie^2v_F}{3\pi J\hbar}}, \tag{39}$$

which changes with distance d. For the separation $d = 100a_0$, this expression gives $\delta_C = 460$ meV, which is remarkably close to 500 meV, i.e., the damping parameter used to fit the

Drude friction curve in Fig. 9(b). Such behavior is therefore an artifact, as it should be, because the linear terms in S in Eqs. (35) and (37) arise from different physical origins: in the Drude spectrum, it is the long plasmon tail (due to a very large damping constant), as compared to the continuum of electron-hole excitations in Eq. (35). Nevertheless, this opens a possibility to fit the experimental results using the Drude model with a different damping constant (39) for each distance d, even if this is not justified. On the other hand, no adjustment of the Drude model expressions would be able to reproduce oscillations [red solid line in Fig. 9(b)] that arise from the quantum size effects.

V. CONCLUSION

In this paper, we provide a new microscopic derivation of energy dissipation rate and friction force between two parallel slabs moving at constant velocity. We confirm the original theoretical results by Pendry,[14,19] but generalize them to include nonlocal effects, in particular excitation of electron-hole pairs. We compare this formulation to two local models for the surface reflectivity and show that a fully nonlocal approach is necessary to describe the behavior of low velocity friction, which is dominated by the low Q electron-hole excitations.

This conclusion remains valid even when additional dissipation is phenomenologically included in the nonlocal calculation of electronic response, as discussed in Sec. IV B.

Therefore, our theory generalizes previous results for the energy dissipation and quantum (or van der Waals) friction, in a way which is similar to our generalization of the theory of van der Waals and Casimir energies.[24,26] However, there is one important difference between these two phenomena: nonlocal effects give only corrections to the local results for the van der Waals–Casimir energy, which arises mainly from the virtual exchange of surface plasmons or polaritons, while in the friction, as we have seen, nonlocal description is essential because it enables us to include contribution of electron-hole excitations, which is the dominant mechanism of friction at low velocities.

The main contribution of this paper is that it provides a method for the microscopic calculation of surface reflectivities, based on the self-consistently calculated electronic wave functions, from which we obtain nonlocal response functions and also smooth, charge-density profiles at surfaces, without resorting to any matching procedure or Fresnel formulas.

ACKNOWLEDGMENTS

Two of the authors (V.D. and M.Š.) are grateful for the hospitality at the Donostia International Physics Center where this work was finalized, and for useful discussions with J. Pendry, A. A. Lucas, and M. S. Tomaš. One of us (V.D.) acknowledges the support of the University of the Basque Country and the Spanish Ministerio de Ciencia y Technologia.

[1] R. Nunez, P. M. Echenique, and R. H. Ritchie, J. Phys. C **13**, 4229 (1980).
[2] T. L. Ferrell, P. M. Echenique, and R. H. Ritchie, Solid State Commun. **32**, 419 (1979).
[3] T. L. Ferrell and R. H. Ritchie, Phys. Rev. A **21**, 1305 (1980).
[4] J. F. Annett and P. M. Echenique, Phys. Rev. B **34**, 6853 (1986).
[5] V. M. Silkin, M. Alducin, J. I. Juaristi, E. V. Chulkov, and P. M. Echenique, J. Phys. Condens. Matter **20**, 304209 (2008).
[6] M. Alducin, V. M. Silkin, J. I. Juaristi, and E. V. Chulkov, Phys. Rev. A **67**, 032903 (2003).
[7] E. Buks and M. L. Roukes, Phys. Rev. B **63**, 033402 (2001).
[8] H. B. Chan, V. A. Aksyuk, R. N. Kleiman, D. J. Bishop, and Federico Capasso, Science **291**, 1941 (2001).
[9] H. B. Chan, V. A. Aksyuk, R. N. Kleiman, D. J. Bishop, and Federico Capasso, Phys. Rev. Lett. **87**, 211801 (2001).
[10] V. Teodorovich, Proc. R. Soc. London Ser. A **362**, 71 (1978).
[11] W. L. Schaich and J. Harris, J. Phys. F **11**, 65 (1981).
[12] L. S. Levitov, Europhys. Lett. **8**, 499 (1990).
[13] V. E. Mkrtchian, Phys. Lett. A **207**, 299 (1995).
[14] J. B. Pendry, J. Phys. Condens. Matter **9**, 10301 (1997).
[15] B. N. J. Persson and Z. Zhang, Phys. Rev. B **57**, 7327 (1998).
[16] A. I. Volokitin and B. N. J. Persson, Rev. Mod. Phys. **79**, 1291 (2007).
[17] A. I. Volokitin and B. N. J. Persson, Phys. Rev. Lett. **106**, 094502 (2011).
[18] A. I. Volokitin and B. N. J. Persson, Phys. Rev. B **78**, 155437 (2008).
[19] J. B. Pendry, New J. Phys. **12**, 033028 (2010).
[20] T. G. Philbin and U. Leonhardt, New J. Phys. **11**, 033035 (2009).
[21] U. Leonhardt, New J. Phys. **12**, 068001 (2010).
[22] J. B. Pendry, New J. Phys. **12**, 068002 (2010).
[23] A. I. Volokitin and B. N. J. Persson, J. Phys. Condens. Matter **11**, 345 (1999).
[24] V. Despoja, M. Šunjić, and L. Marušić, Phys. Rev. B **75**, 045422 (2007).
[25] L. Marušić, V. Despoja, and M. Šunjić, J. Phys. Condens. Matter **18**, 4253 (2006).
[26] V. Despoja, M. Šunjić, and L. Marušić, Phys. Rev. B **83**, 165421 (2011).
[27] Z. Penzar and M. Šunjić, Phys. Scr. **30**, 431 (1984).
[28] L. Marušić and M. Šunjić, Phys. Scr. **63**, 336 (2001).